Copper phosphide and persulfate salt: A novel catalytic system for the degradation of aqueous phase micro-contaminants

Charalampia Alexopoulou, Athanasia Petala, Zacharias Frontistis, Charalampos Drivas, Stella Kennou, Dimitris I. Kondarides, Dionissios Mantzavinos*

Department of Chemical Engineering, University of Patras, Caratheodory 1, GR-26504, Patras, Greece

A B S T R A C T

The heterogeneous activation of sodium persulfate (SPS) using copper (I) phosphide (Cu_3P) nanoparticles was tested in this work. The catalyst was synthesized via a two-step method involving preparation of $Cu(OH)_2$ and subsequent low temperature phosphidation and characterized with BET, XRD, TEM/HRTEM, SEM and XPS techniques. The XRD pattern showed the existence of hexagonal Cu_3P phase with mean primary crystallite size of *ca.* 28 nm. The XP spectra indicated the presence of residual $Cu(OH)_2$ and $Cu_3(PO_4)_2$ species on the catalyst surface, originating from the synthesis methods employed, which disappeared after exposure to reaction conditions.

The activity of Cu_3P was evaluated for the degradation of antibiotic sulfamethoxazole (SMX), which occurred in short reaction times. The effect of catalyst concentration (20–80 mg/L), SPS dosage (0.05–1 g/L) and SMX concentration (0.5–4.1 mg/L) on degradation was studied. Results obtained in ultrapure water (UPW) showed that SMX degradation increases with increasing catalyst content in the range 20–80 mg/L and SPS concentration in the range 0.05–0.5 g/L. In contrast, increasing SPS concentration at 1 g/L leads to lower reaction rates. Experiments were also conducted in bottled water, secondary treated wastewater, UPW spiked with bicarbonate or chloride ions, as well as UPW containing humic acid. With the use of t-butanol and methanol as radical quenching agents, $SO_4^{\bullet-}$ was found to be the primary radical species responsible for SMX degradation. The simultaneous use of Cu_3P and solar irradiation as persulfate activators resulted in a synergistic effect in experiments performed in UPW and wastewater.

From a mechanistic point of view, Cu_3P acts as an electron mediator or bridge to facilitate the electron-transfer processes and this is accompanied by the intermediate formation of radicals. The catalyst remains intact, thus implying the catalytic nature of the process.

1. Introduction

Sulfate radical ($SO_4^{\bullet-}$) holds a prominent position among various reactive oxygen species (ROS) incorporated in advanced oxidation processes (AOPs) [1]. Equal or even higher redox potential (2.5–3.1 V vs NHE, pH ~ 6), longer lifetime (30–40 μs) and wider pH range (2–9) of operation, in comparison with hydroxyl radicals (˙OH), are the main reasons for $SO_4^{\bullet-}$ popularity [2,3]. Moreover, $SO_4^{\bullet-}$ reacts with target organic contaminants in different ways than ˙OH, providing a more effective alternative degradation mechanism [4,5], and maintains its high oxidation efficiency in carbonate and phosphate solutions which is of higher environmental significance than ultrapure water [6]. In all cases, $SO_4^{\bullet-}$ can further react generating other oxidative radicals, such as ˙OH. Moreover, the final product of persulfate conversion is the

sulfate anion, whose concentration in discharged waters is acceptable up to 250 mg/L [7].

While non-activated persulfate is characterized by low oxidation ability, it can be successfully activated via heat [8], ultraviolet (UV) light [9], transition metal ions [10], alkali [11], chemicals [12] and heterogeneous activators [13], resulting in the formation of the highly active $SO_4^{\bullet-}$ radical. In recent years, many non-conventional activators have been investigated, including activated carbon [14], by-products of water treatment plants [15], electrochemical method [16], ultra-sonication [17], γ-rays [18] electron beam [19], as well as combinations of the above.

Transition metal cations (Co^{2+}, Mn^{2+}, Ni^{2+}, Fe^{2+}, Ru^{3+}, Ce^{3+}) are considered suitable persulfate activators in decontamination processes, due to the relatively low energy demands, low operational costs, high

performance and ease of operation of such systems. In particular, most of the studies have focused on Co^{2+}/peroxymonosulfate (PMS) systems, as they have shown the highest activity for pollutants degradation even in neutral pH [20]. However, homogeneous transition metals/persulfate systems suffer from some important limitations. At the end of the oxidation process the effluent contains metal ions at concentrations far from the environmental tolerance limits for drinking water [21], making necessary the use of a subsequent separation/recovery step. This additional step not only increases the cost but also the complexity of the overall process. Additionally, transition metal species are highly affected by the pH and composition of aqueous matrices, which most of the times decrease their performance [2].

To overcome these problems, recent research efforts aim at developing heterogeneous transition metal-based catalysts as alternative persulfate activators [21]. Solid activators are more stable, cost-effective and easy to recover, through e.g. filtration or centrifugation. The majority of heterogeneous catalysts are based on cobalt compounds [21]. Co_3O_4 itself or supported on various materials has been successfully adopted as heterogeneous activator in water treatment processes [22], with the oxidation mechanism being similar to the one reported for homogeneous Co^{2+} systems [23,24].

Apart from cobalt compounds, copper oxides (CuO, Cu_2O) have been recently considered as suitable heterogeneous activators for persulfate or PMS. In the case of copper, two contradicting views on the degradation mechanism have been reported [25,26]. Zhang et al. proposed a non-radical mechanism for the CuO/persulfate system [25], while Lei et al. found that phenol degradation in $CuO-Fe_3O_4$/persulfate involved the formation of $SO_4^{\cdot-}$ and $\cdot OH$ radicals [26]. A follow-up study on CuO/persulfate system reconciled previous findings and suggested that both radical and non-radical mechanisms may occur, whose relative significance depends on the specific operating conditions in question [27]. However, it should be noted that the Cu-based heterogeneous activators investigated so far are limited to CuO_x formulations.

Copper (I) phosphide (Cu_3P) belongs to the group of transition metal phosphides represented by the general formula M_xP_y [28]. Cu_3P is widely used as catalyst in hydrodesulfurization reaction and as anode material for lithium ions batteries [29,30]. Moreover, it has been adopted as electrocatalyst [31] resulting in high hydrogen evolution reaction rate and as co-catalyst in photocatalytic hydrogen production reactions [32–34]. Very recently, Luo et al. presented a CoP/PMS system for removal of organic contaminants, which achieved superior activity than the most-reported Co_3O_4/PMS system [35].

The main goal of the present study is to investigate, for the first time, the applicability of Cu_3P as heterogeneous sodium persulfate (SPS) activator for the degradation of the antibiotic agent sulfamethoxazole (SMX). SMX is a model compound representing the pharmaceuticals and personal care products (PPCPs) group of emerging micro-contaminants. Experimental parameters such as catalyst loading, initial SMX and SPS concentration and the effect of water matrix are investigated. Synergistic effects, arising from the simultaneous use of solar irradiation, are also studied. Mechanistic considerations, based on catalyst characterization and degradation kinetics, are also discussed.

2. Experimental

2.1. Chemicals and water matrices

For catalyst preparation, copper (II) nitrate trihydrate (Cu $(NO_3)_2 \cdot 3H_2O$, CAS:10031-43-3) and sodium hypophosphite monohydrate ($NaH_2PO_2 \cdot H_2O$, CAS: 10039-56-2) were supplied by Alfa Aesar, tri-sodium citrate dihydrate ($Na_3C_6H_5O_7 \cdot 2H_2O$, CAS: 6132-04-3) and ammonia solution 25% (NH_4OH, CAS: 1336-21-6) were purchased from Sigma Aldrich and sodium hydroxide (NaOH, CAS: 1310-73-2) from Penta.

Sulfamethoxazole ($C_{10}H_{11}N_3O_3S$, CAS: 723-46-6) and sodium persulfate ($Na_2S_2O_8$, CAS: 7775-27-1), t-butanol ($C_4H_{10}O$, CAS: 75-65-0),

methanol (CH_3OH, CAS: 67-56-1), humic acid (HA, CAS: 1415-93-6), sodium chloride (NaCl, CAS: 7647-14-5), sodium bicarbonate ($NaHCO_3$, CAS: 144-55-8) and acetonitrile (CH_3CN, CAS: 75-05-8, for HPLC analysis) were obtained from Sigma-Aldrich. Potassium iodide (KI, CAS: 7681-11-0) was purchased from Carlo Erba reagents. All chemicals were used as received, without further purification.

Most experiments were conducted in ultrapure water (UPW), while secondary effluent from the University of Patras campus wastewater treatment plant (WW) and commercial bottled water (BW) were also used. Details about water matrices can be found elsewhere [36,37].

2.2. Preparation of copper (I) phosphide (Cu_3P)

The Cu_3P powder was synthesized through a two-step method involving preparation of $Cu(OH)_2$ and subsequent low-temperature phosphidation [31,32]. In detail, 200 mg of $Cu(NO_3)_2 \cdot 6H_2O$ was dissolved in 100 mL aqueous solution containing 50 mg $NaH_2PO_2 \cdot H_2O$ under stirring. Appropriate amount of NH_4OH 25% aqueous solution was added drop-wise to the mixture until the muddy solution turned clear. An excess amount of NaOH aqueous solution (0.5 M) was then added to the above mixture until sediments were formed. The resulting material was collected by filtration, washed with deionized water and dried at 60 °C under vacuum to obtain $Cu(OH)_2$. Afterwards 50 mg of the obtained $Cu(OH)_2$ and 250 mg of $NaH_2PO_2 \cdot H_2O$ were mixed together and grounded in a mortar to form a fine powder. Then, the mixture underwent thermal treatment in N_2 atmosphere at 300 °C for 1 h. The system was cooled down at room temperature under N_2 flow. The as obtained dark grey-black powder was washed with deionized water for several times and dried at 60 °C for 12 h.

2.3. Catalyst characterization

X-ray diffraction (XRD) analysis was performed using a Brucker D8 Advance Instrument equipped with a Cu Kα source operated at 40 kV and 40 mA. The diffraction patterns were recorded in the range 10° to 80°. The phase identification was based on JCPDS cards. The average primary crystallite size was estimated using the Scherrer equation [38]. Specific surface area (SSA) of the sample was determined with the Brunauer-Emmett-Teler (BET) method with the use of a Micromeritics (Gemini III 2375) instrument, employing nitrogen physisorption at the temperature of liquid nitrogen (−196 °C). Pore volume and pore diameter of the sample were determined following the Barret-Joyner-Halenda (BJH) method. High resolution transmission electron microscopy (HRTEM) images were obtained using a JEOL JEM-2100 system, operated at 200 kV (point resolution 0.23 nm), while scanning electron microscopy (SEM) images were obtained using a JEOL 6300 scanning electron microscope equipped with an energy dispersive spectrometer (EDS) for the elemental analysis of the sample.

X-ray photoelectron spectroscopy (XPS) measurements were carried out using unmonochromatized Al Ka line at 1486.6 eV (12 kV with 20 mA anode current) and a Leybold EA-11 analyzer with constant pass energy of 100 eV. The analyzed area was approximately a 2×5 mm^2 rectangle, positioned near the geometric center of each sample. XPS analysis was carried out at a 0 degrees take-off angle (normal to the sample area). In all XP spectra, the binding energy (BE) of the predominant aliphatic contribution to the C 1 s peak at 284.8 eV was used as a measured BE reference.

2.4. Experimental procedure and analytical methods

Experiments were carried out in a cylindrical pyrex reaction vessel of 250 mL capacity open to the atmosphere. A solution of 120 mL containing the desired SMX concentration was loaded in the vessel and pre-weighted amounts of SPS and Cu_3P were then added. Experiments were conducted under continuous magnetic stirring at ambient temperature and inherent solution pH.
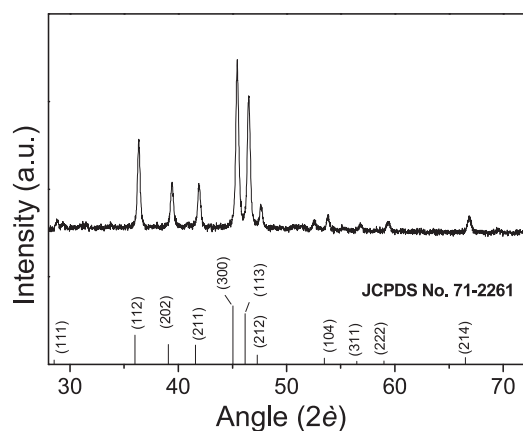
Fig. 1. X-ray diffraction pattern of the as prepared catalyst. The JCPDS card for the hexagonal structure of Cu_3P is also shown for comparison.

Samples of 1.2 mL were withdrawn from the vessel at desired time periods, quenched with methanol, filtered and analyzed by high performance liquid chromatography (HPLC) using an Alliance HPLC system consisting of a photodiode array detector (Waters 2996), a gradient pump (Waters 2695) and a Kinetex column (C18 100 A, 150 mm × 3 mm; 2.6 μm particle size) maintained at 45 °C. The mobile phase consisted of 68:32 water:acetonitrile, while the injection volume was 40 μL.

Persulfate was measured spectrophotometrically at 352 nm (HACH DR5000) following its reaction with iodide [39].

A solar simulator (Oriel, model LCS-100) equipped with a 100 W Xenon (ozone free) lamp was employed to study the combined activation of persulfate by Cu_3P and light irradiation.

3. Results and discussion

3.1. Characteristics of Cu_3P catalyst

The XRD pattern of Cu_3P is shown in Fig. 1. It is observed that all peaks can be ascribed to the hexagonal phase of Cu_3P (JCPDS No 7 1-2 261) [31,40]. The mean primary crystallite size of Cu_3P was estimated according to the Scherrer equation based on the X-ray line broadening of the (300) peak located at $2\theta = 45.4°$ and it was found to be ~ 28 nm. According to the BET method, the specific surface area of Cu_3P powder is ~ 4 m²/g, while pore volume and average pore diameter are 0.0069 cm³/g and 127 Å, respectively.

Fig. 2A shows a characteristic SEM image of Cu_3P. It is observed that the sample consists of relatively small and uniform spherical-shaped aggregates with an average size of *ca.* 150 nm, as measured with the "Image J" software. EDS mapping (Fig. 2B) shows the presence of homogeneously distributed Cu (red symbols) and P (green symbols) elements, while the EDS spectrum of this SEM image (inset in Fig. 2B) confirms the absence of impurities. The morphology of the catalyst was further examined using HRTEM and the results are shown in Fig. 2C. It is observed that the interplanar spacing of 0.25 nm matches with the (112) lattice plane of Cu_3P. Moreover, characteristic diffraction rings indexed to Cu_3P are identified in the corresponding SAED pattern shown in Fig. 2D.

3.2. Catalytic activity

The degradation of 0.5 mg/L SMX in UPW as function of time using Cu_3P at different concentrations (20–80 mg/L) is illustrated in Fig. 3A. Considering that SMX degradation follows pseudo-first-order kinetics, the reaction rate can be calculated from the following equation for n = 1 [41]:

$$rate = -\frac{d[SMX]}{dt} = k_{app}[SMX]^n \tag{1}$$

Apparent rate constants (k_{app}) were calculated from the linearized form of Eq. (1) and are shown in brackets. Fig. 3A also shows results of a blank experiment conducted in the absence of catalyst. It is observed that less than 10% of SMX was degraded in the latter case after 30 min, indicating that SPS cannot be activated in the absence of catalyst at ambient conditions. With the addition of only 20 mg/L Cu_3P, about 60% of SMX was removed in the same period, while 40 mg/L Cu_3P led to complete degradation of SMX in *ca.* 20 min, as more active sites are available for SPS activation [42]. The apparent rate constant increased from 0.030 min^{-1} for 20 mg/L Cu_3P to 0.114 min^{-1} for 40 mg/L Cu_3P. Further increase of Cu_3P concentration to 80 mg/L resulted in an increase of k_{app} to 0.200 min^{-1}. Fig. 3A also shows an experiment with spent catalyst at 40 mg/L (dashed line). Following its usage, the catalyst was separated from the reaction mixture, washed-out with water, dried and then re-used; as clearly seen in Fig. 3A, SMX concentration profiles are identical for the experiments with the fresh and the spent sample.

The effect of initial SPS concentration on the degradation rate was investigated in the range of 0.05–1.00 g/L in the presence of 40 mg/L Cu_3P. As seen in Fig. 3B, when the SPS concentration increases from 0.05 g/L to 0.5 g/L the required time for complete SMX degradation is halved, and the apparent constant increases from 0.061 to 0.226 min^{-1}. Further increase of SPS concentration resulted in decreased degradation efficiency, probably due to the fact that excess amount of SPS could scavenge radicals, thus reducing the degradation rate [43–45]. At the same time, SMX removal due to adsorption (i.e. in the absence of persulfate) is limited to almost 13% after 30 min.

Wu et al. [46], who studied the degradation of 0.3 mg/L SMX by magnetite-activated persulfate, reported a k_{app} value of about 0.005 min^{-1} at 300 mg/L Fe_3O_4 and 240 mg/L persulfate; these values are 1–2 orders of magnitude lower than those reported in Fig. 3. Experiments were also conducted at various magnetite concentrations between 300 and 2000 mg/L and persulfate concentrations between 48 and 480 mg/L; the rate of degradation was found to increase with increasing catalyst or oxidant concentration up to a threshold value, beyond which inhibitory effects occurred. Du et al. [47] studied persulfate activation by several, commercially available, zero-valent iron samples for SMX degradation; they reported k_{app} values between 0.00 and 0.25 min^{-1} (depending on the catalyst sample) for the degradation of 5.1 mg/L SMX with 56 mg/L Fe° and 240 mg/L persulfate. In other studies [48], Chen and Carroll tested N-doped graphene for the activation of SPS; they reported complete removal of 5 mg/L SMX after 180 min of reaction with 50 mg/L catalyst and 240 mg/L SPS. Zhu et al. [49] studied SMX degradation with N-doped biochars capable of activating persulfate and reported about 60% degradation of 50 mg/L SMX after 60 min of reaction with 200 mg/L catalyst and 480 mg/L persulfate. Our group has recently investigated [50] the use of biochars of agro-industrial origin for the activation of SPS and subsequent degradation of SMX; a k_{app} value of 0.03 min^{-1} was recorded for the degradation of 0.25 mg/L SMX with 90 mg/L biochar and 250 mg/L SPS. Details of the aforementioned studies [46–50] regarding the degradation of SMX by heterogeneous catalysts activating SPS are given in Table 1.

To investigate the effect of initial SMX concentration on reaction kinetics, a set of experiments were conducted varying SMX concentration from 0.5 to 4.1 mg/L. Results are depicted in Fig. 4, where SMX conversion (%) and k_{app} (min^{-1}) are shown as function of SMX concentration (mg/L). It is observed that for SMX concentrations in the range 0.5–1.0 mg/L both k_{app} and conversion are independent of the initial SMX concentration showing that the reaction follows first-order kinetics. However, an increase of SMX concentration from 1.0 to1.5 mg/L results in a decrease in k_{app} from 0.124 to 0.057 min^{-1} implying a transition from first to zeroth-order kinetics, i.e. Eq. (1) for n = 0 [51]. Further increase in SMX concentration to 4.1 mg/L results in a decrease
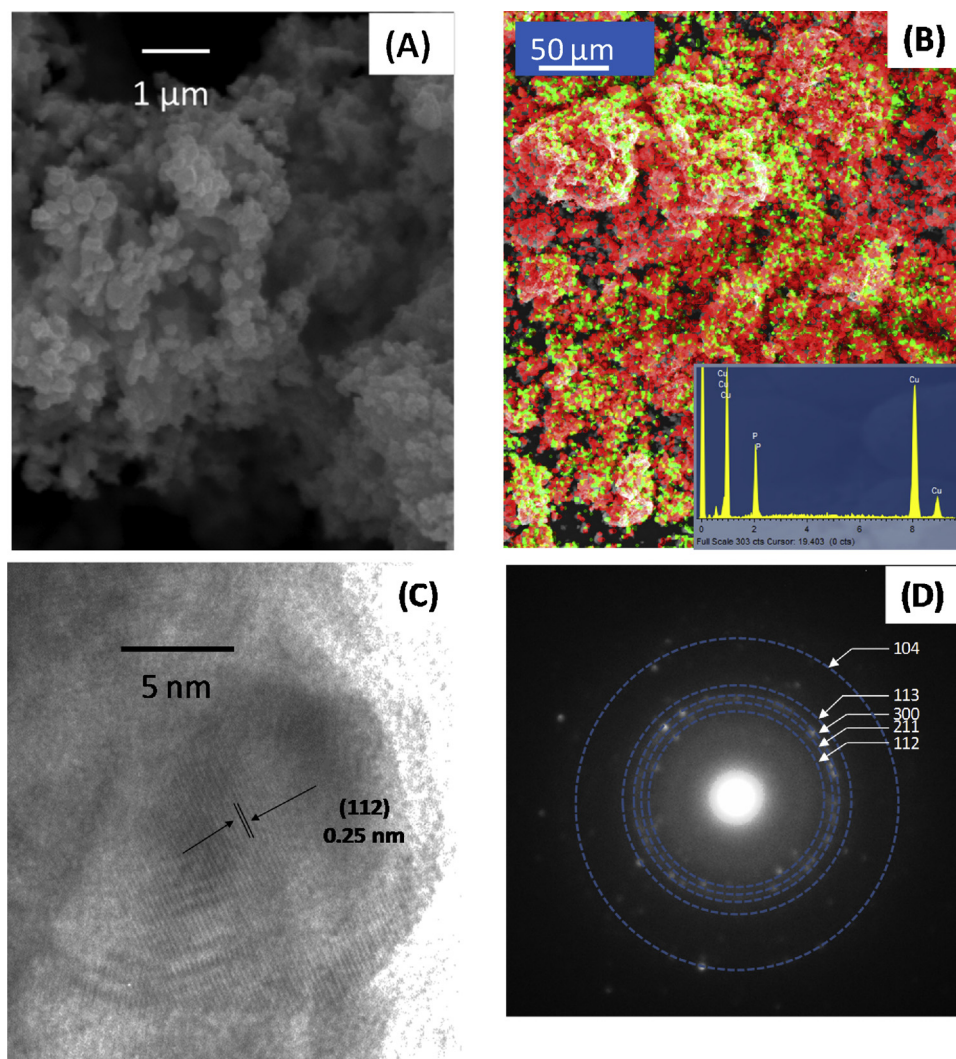
Fig. 2. (A) SEM image of the as prepared Cu_3P catalyst. (B) EDS mapping results showing the distribution of Cu (red symbols) and P (green symbols). Inset: EDS spectrum obtained from this SEM image. (C) HR-TEM image of Cu_3P. (D) Typical SAED pattern of Cu_3P nanoparticles. (For interpretation of the references to colour in this figure legend, the reader is referred to the web version of this article).

in conversion from 55% to 25%.

The water matrix effect is probably the most crucial parameter affecting the performance of AOPs, as aqueous matrices of environmental significance consist of a great number of organic and inorganic substances that can interfere with the target pollutant, thus either promoting or suppressing the efficiency of the process. In order to investigate the effect of the water matrix in different concentration of ROS on SMX degradation, experiments were conducted at two SPS concentrations (0.1 and 0.5 g/L), for the case of bottled water (BW) and secondary treated wastewater (WW) and results are presented in Fig. 5. At 0.5 g/L SPS, SMX in UPW is completely degraded after 15 min; however, degradation decreases to 35% and 19% in BW and WW, respectively. The same trend is observed at the lower SPS concentration of 0.1 g/L, with longer times required for the degradation of SMX. Fig. 5 clearly shows that the presence of inorganic ions in BW has a considerable negative impact on the degradation of SMX, resulting in lower reaction rates, while the effect is more pronounced in the case of WW, containing additional organic matter.

To further understand the hampering role of BW and WW, additional experiments were conducted, where bicarbonate ions (HCO_3^-) (100 or 250 mg/L, this concentration range was selected to match typical values in BW samples in Greece) or chloride ions (Cl^-) (50 or 100 mg/L, values that are typical of groundwater taken from the

University campus boreholes), which are the dominant ions in natural waters and in BW, were added in UPW. Usually, the presence of Cl^- in water matrix results in lower degradation rates, as Cl^- reacts with $SO_4^{\bullet-}$ producing less reactive chlorine radicals ($Cl^\bullet$, $Cl_2^{\bullet-}$, $ClOH^{\bullet-}$) [52]. Interestingly, the presence of 50 mg/L Cl^- does not affect appreciably the degradation rate, while higher amounts of Cl^- lead to a relatively small decrease of the degradation rate (Fig. 6A). This can be attributed to the enhanced formation of $^\bullet OH$ induced by Cl^- [1], as well as to the high reactivity of chlorine radicals with electron-rich compounds [53].

On the other hand, addition of HCO_3^- in UPW has a detrimental effect on the degradation rate (Fig. 6A). Both HCO_3^- concentrations tested in the present work resulted in a decrease of k_{app} from 0.114 min^{-1} for UPW to 0.032 min^{-1}. The dominant reason for the lowering of k_{app} is probably the effective scavenging of the highly reactive $SO_4^{\bullet-}$ and $^\bullet OH$ radicals by HCO_3^- ions, producing the secondary reactive carbonate radicals ($HCO_3^\bullet$) [1,53,54]. Generally, the way that the bicarbonate and chloride anions react with $SO_4^{\bullet-}$, $^\bullet OH$ and with the organic pollutant is complicated and not clearly understood [55]. Additionally, functional parameters such as pH, SPS dosage and the nature of the organic contaminant seem to affect this complex reaction network, resulting in a great amount of conflicting views existing in the literature.

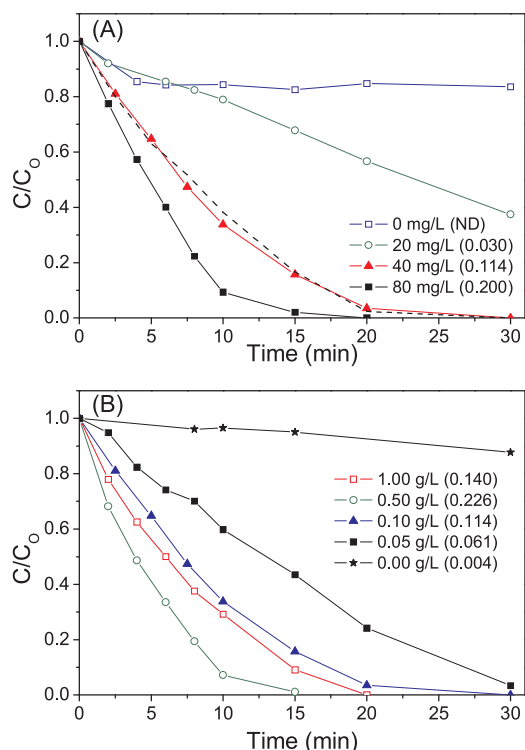Fig. 6A also shows the SMX degradation profile obtained in the

Fig. 3. Effect of (A) Cu_3P concentration (0.1 g/L SPS) and (B) SPS concentration (40 mg/L Cu_3P) on the degradation of 0.5 mg/L SMX in UPW. Numbers in brackets show apparent rate constants in min^{-1} according to Eq. (1). ND: not determined. Dashed line in (A) shows experiment with 40 mg/L spent catalyst.

presence of humic acid in UPW. HA is an organic molecule that represents the organic fraction naturally occurring in waters. Interestingly, while most of the relevant studies mention an inhibitory effect of HA [36,56], it is observed that the addition of 10 mg/L HA has practically no effect on the reaction rate. These results are consistent with results reported by Fang et al. [57], who found that the addition of HA resulted in the formation of higher amounts of $SO_4^{\bullet-}$ and $^{\cdot}OH$ radicals in the solution, as measured with the use of electron paramagnetic resonance (EPR) technique. Based on the above, it is concluded that the observed deterioration of catalytic performance in BW and WW (Fig. 5) is mainly due to the presence of HCO_3^- ions.

As already mentioned, it is believed that the radical species responsible for SMX degradation are $SO_4^{\bullet-}$ and $^{\cdot}OH$. In order to clarify which of these radicals has the dominant role in the present reaction system, excess amounts of appropriate scavenging agents were adopted, and results are shown in Fig. 6B. It is observed that in the presence of 5 g/L t-BuOH, k_{app} decreases from 0.114 to 0.056 min^{-1}. As reported previously [10], t-BuOH reacts effectively with $^{\cdot}OH$ and very slowly with $SO_4^{\bullet-}$. Indeed, the reaction rate of t-BuOH with $^{\cdot}OH$ ($3.8 \times 10^8 - 7.6 \times 10^8$ $M^{-1}s^{-1}$) is 1000-fold greater than that with $SO_4^{\bullet-}$ ($4 \times 10^5 - 9.1 \times 10^5$ $M^{-1}s^{-1}$) [10]. On the contrary, addition of 5 g/L MeOH had significant influence on SMX removal. MeOH can quench both $^{\cdot}OH$ and $SO_4^{\bullet-}$ with rate constants of $1.2–2.8 \times 10^9$ $M^{-1}s^{-1}$ and $1.6–7.7 \times 10^7$ $M^{-1}s^{-1}$, respectively [58]. Relying on the above results, $SO_4^{\bullet-}$ are considered as the dominant species for SMX degradation in the present system.

3.3. Coupling Cu_3P with solar irradiation for SPS activation

In order to examine the existence of synergistic effects on SPS activation, additional experiments were carried out under simulated solar irradiation in both UPW and WW (Fig. 7). It should be noted that the SPS dosage in WW was higher (0.5 g/L) than in UPW (0.1 g/L) in order

Table 1
Studies of SMX degradation with SPS activated by heterogeneous catalysts.

| SMX	Catalyst	Oxidant source	Performance	Reference
0.3 mg/L	300–2000 mg/L Fe_3O_4	48–480 mg/L SPS	Degradation increases with increasing catalyst in the range 300–1000 mg/L but decreases thereafter. Optimum SPS concentration at 360 mg/L. Best results at pH = 3.5. At acidic conditions, chloride ions can act as sulfate radical scavengers. Hydroxyl radicals are the main oxidant species.	[46]
5.1 mg/L	56 mg/L Fe° (eight samples with 4–90 μm particle size, 0.1–1.1 m^2/g BET area and >95 wt% iron)	240 mg/L SPS or 3.4 mg/L H_2O_2	Degradation depends on the catalyst and is enhanced in the presence of a weak magnetic field. Best results at pH = 3–4. Iron leaching occurs. Interactions of sulfate radicals with nitrate and chloride anions form respective radicals. Reaction pathways based on hydroxyl and sulfate radicals are proposed.	[47]
5 mg/L	50 mg/L N-doped graphene (N-GP) or aminated graphene (NH_2-GP) or graphene oxide (GO)	240 mg/L SPS	Reactivity decreases in the order: N-GP > NH_2-GP > > GO. Alkaline conditions (pH = 9) favor degradation with N-GP but impede it with NH_2-GP. Variable effect of the water matrix (bicarbonate, chloride and sulfate anions, humic acid) depending on the catalyst. Evidence of a non-radical activation mechanism.	[48]
50 mg/L	200 mg/L N-doped biochar prepared from reed biomass annealed at 400–900 °C	480 mg/L SPS	Biochar activity is affected by annealing temperature (optimum at 900 °C resulting in biochar with 497 m^2/g BET area). Tests also performed with azodye, phenol and bisphenol. Non-radical mechanisms dominate over radical reactions.	[49]
0.125–0.5 mg/L	90 mg/L biochar prepared by spent malt rootlets annealed at 900 °C	100–250 mg/L SPS	Degradation increases with increasing SPS and decreasing SMX concentration. Best results at acidic environment. Neither the water matrix (bottled water or wastewater) nor radical scavengers (alcohols) affect degradation. Evidence of reactions with radicals trapped onto the biochar surface. Synergistic enhancement of degradation occurs when ultrasound or solar light irradiation is applied.	[50]
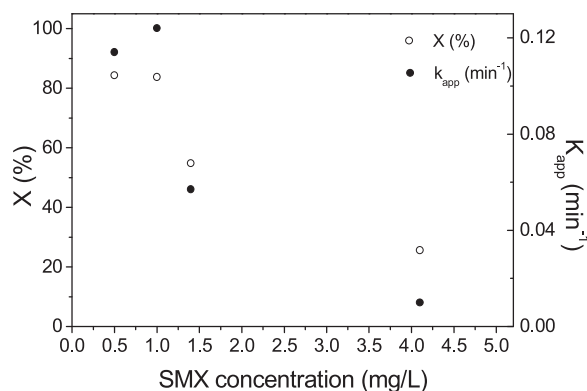
Fig. 4. Effect of initial SMX concentration on 15-min conversion (left axis) and apparent rate constant (right axis) with 40 mg/L Cu$_3$P and 0.1 g/L SPS in UPW.
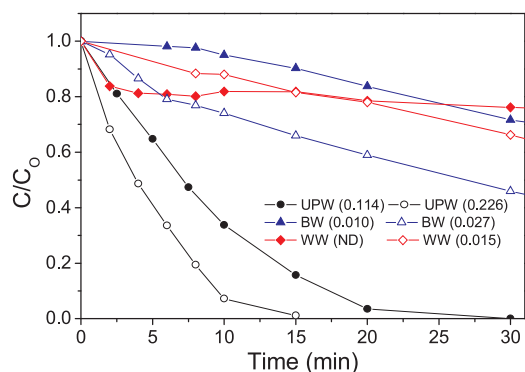

Fig. 5. Effect of the water matrix on 0.5 mg/L SMX degradation with 40 mg/L Cu$_3$P and 0.1 g/L (filled symbols) or 0.5 g/L (open symbols) SPS. Numbers in brackets show apparent rate constants in min^{-1} according to Eq. (1). ND: not determined.

to balance the inhibitory phenomena occurring in WW.

In UPW (Fig. 7A), the value of k$_{app}$ for the SPS/solar light pair was only 0.010 min^{-1}, indicating a minor activation of SPS by solar irradiation. Persulfate can be activated by UV light, whose wavelength has a significant impact on the quantum yields of sulfate radicals; the yield decreases as the wavelength shifts from UV-C to UV-A [2]. The dominant mechanism of SPS activation is thought to be the splitting of its O−O bond from the energy input of UV light [2]. Given that the solar spectrum contains only ca 6% UV-A, the relatively low activation by solar irradiation is not surprising. With the addition of 40 mg/L Cu$_3$P, k$_{app}$ increased significantly to 0.222 min^{-1}, while the k$_{app}$ value for the SPS/Cu$_3$P pair in the dark was 0.114 min^{-1}. The fact that the sum of the rate constants of the individual processes (0.124 min^{-1}) is lower than that of the combined process (0.222 min^{-1}) suggests the existence of synergistic rather than cumulative effects in the present system [55]. Notably, photolysis in the absence of catalyst and oxidant does not contribute to SMX degradation.

Qualitatively similar trends were observed for the experiments conducted in WW (Fig. 7B) although the degradation rates were always lower than in UPW. For the SPS/solar light pair, the k$_{app}$ value was 0.003 min^{-1}; however, when SPS was activated by solar irradiation and Cu$_3$P simultaneously, 100% SMX degradation was achieved within 45–60 min. In the same period, degradation reached only 75% for the SPS/Cu$_3$P pair in the dark. Eq. (2) can be used to quantify the extent of synergy, S, where k_i is the rate constant of each individual process and $k_{combined}$ is the rate constant of the combined process:

$$S(\%) = 100\frac{k_{combined} - \sum_1^n k_i}{k_{combined}}$$
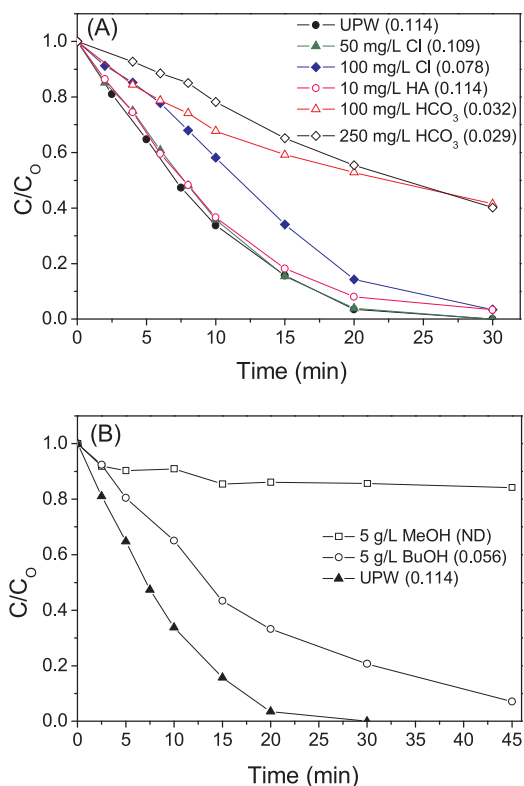
(2)

Fig. 6. Effect of (A) water matrix species and (B) radical scavengers on 0.5 mg/L SMX degradation with 40 mg/L Cu$_3$P and 0.1 g/L SPS in UPW. Numbers in brackets show apparent rate constants in min^{-1} according to Eq. (1). ND: not determined.
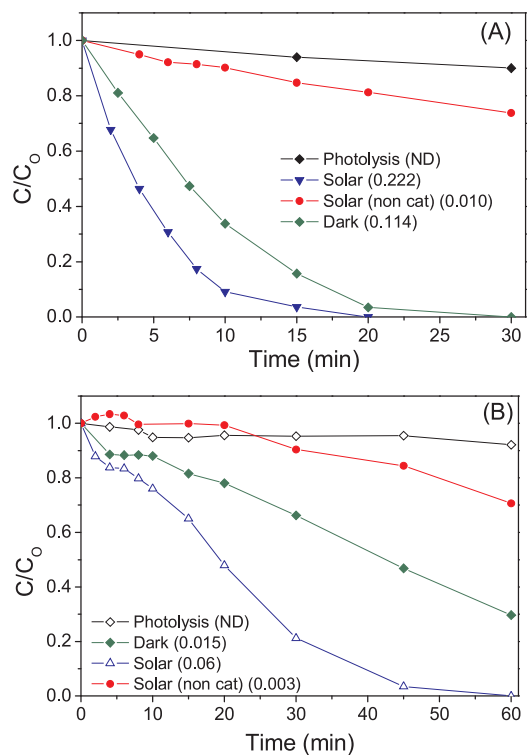

Fig. 7. Synergistic effect of solar irradiation on the degradation of 0.5 mg/L SMX with 40 mg/L Cu$_3$P and (A) 0.1 g/L SPS in UPW or (B) 0.5 g/L SPS in WW. Numbers in brackets show apparent rate constants in min^{-1} according to Eq. (1). ND: not determined.
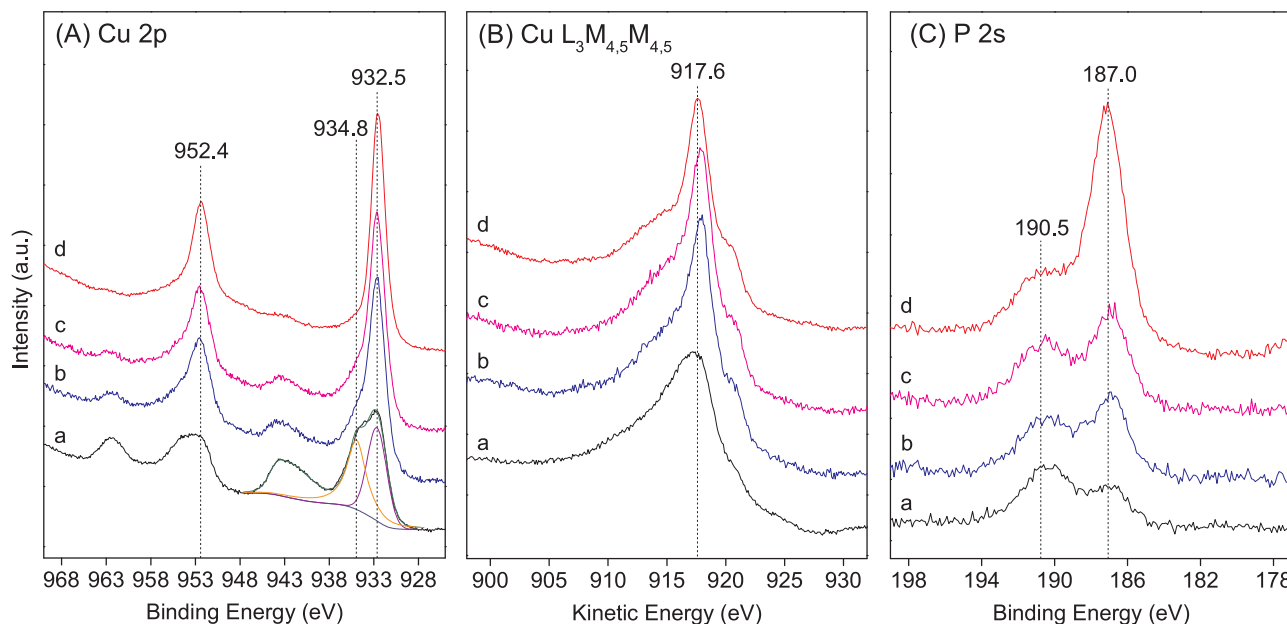
Fig. 8. XP spectra corresponding to (A) Cu 2p, (B) Auger Cu $L_3M_{4,5}M_{4,5}$ and (C) P 2s regions obtained from (a) the fresh catalyst, and from spent catalyst samples collected after exposure to reaction conditions (500 mg/L Cu_3P, 1.2 g/L SPS and 0.5 mg/L SMX) for (b) 4 min, (c) 8 min and (d) 120 min.

Based on the kinetic data shown in Fig. 7, the synergy is 70% in WW and 44% in UPW.

3.4. Surface chemical composition of fresh and spent catalysts

The surface chemical composition of the fresh catalyst, as well as of samples collected after exposure to reaction conditions for different time intervals (4, 8 and 120 min) was investigated *ex situ* by X-ray Photoelectron Spectroscopy (XPS). Experimental conditions for these measurements were: 500 mg/L Cu_3P, 1.2 g/L SPS and 0.5 mg/L SMX.

Results of the XP measurements obtained in the Cu 2p region are shown in Fig. 8A. It is observed that, in all cases, the Cu 2p spectra consist of two main peaks due to spin orbit splitting (S.O.S.), located at 932.5 eV (Cu $2p_{3/2}$) and 952.4 eV (Cu $2p_{5/2}$), and of the corresponding satellites. The presence of these well-known shake-up satellites found in Cu 2p photoelectron spectra is an indication of the existence of Cu^{2+} species on the catalyst surface. However, in the case of the fresh sample (spectrum a), the Cu 2p peaks can be deconvoluted into two components. As seen in Fig. 8A, the main Cu $2p_{3/2}$ feature can be fitted by two peaks located at 932.5 ± 0.1 eV and 934.8 ± 0.1 eV corresponding to Cu^{1+} and Cu^{2+}, respectively. The first peak (Cu^{1+}) is attributed to Cu_3P while the second one to $Cu(OH)_2$ and $Cu_3(PO_4)_2$ [59,60]. Exposure of the catalyst to reaction conditions for few minutes results in an abrupt decrease of the intensity of the 934.8 ± 0.1 eV peak (spectra b, c), indicating the rapid removal of the Cu^{2+} component from the catalyst surface. This is evidenced by the parallel decrease of the intensities of the satellite peaks located at around 943 eV, which appear only in the presence of Cu^{2+} [59], until they disappear for prolonged reaction periods (trace d). The fact that the intensities of the peaks related to Cu^{1+} (e.g. 932.5 ± 0.1 eV) increase at the expense of those related to Cu^{2+} species (e.g. 934.8 ± 0.1 eV) suggests that reduction of surface Cu species occurs during the reaction. It should be noted that results obtained with XRD (Fig. 1), which is a bulk technique, indicated the presence of only Cu_3P in the freshly prepared sample. Since XPS is a surface sensitive technique and its analysis depth is up to *ca.* 10 nm from the surface, it is most probable that the $Cu(OH)_2$ and $Cu_3(PO_4)_2$ species detected in the fresh sample are located on the catalyst surface. These surface species, originating from the catalyst preparation procedure, are rapidly reduced under reaction conditions.

Fig. 8B shows the Auger region of the Cu($L_3M_{4,5} M_{4,5}$), which

corresponds to the main Auger peak. The spectrum obtained for the fresh sample (spectrum a) is characterized by a broad peak, which becomes progressively sharper after exposure of the catalyst to reaction conditions (spectra b–d). The sharp peak recorded after 120 min (spectrum d), which is located at 917.6 eV, can be safely attributed to Cu_3P. In fact, the value of the Auger parameter of this compound, which is characteristic of the chemical bonding, was calculated by the sum of the Cu $2p_{3/2}$ binding energy (BE) and the Cu($L_3M_{4,5} M_{4,5}$) kinetic energy (KE) [61] and was found to be 1850.1 eV, which corresponds to Cu_3P compound. An Auger parameter value for Cu_3P has not been reported until now in the literature.

The XP spectra of the samples obtained in the P 2 s region are shown in Fig. 8C. It is observed that, in all cases, the spectra consist of two discrete peaks located at binding energies of 190.5 ± 0.1 eV and 187.0 ± 0.1 eV, which can be attributed to PO_4 and Cu-P species, respectively [60]. The high BE peak related to PO_4 is more intense for the fresh catalyst (spectrum a). However, exposure of the catalyst to reaction conditions results in a progressive increase of the relative intensity of the low BE peak (spectra b–d) which is the dominant one after 120 min (trace d). These results provide additional evidence that reduction of the surface $Cu_3(PO_4)_2$ species occurs under reaction conditions. Since the area under the photopeaks is proportional to the P atomic concentration on the surface, it turns out that the overall P 2 s area has significantly increased during the reaction implying that the main contribution comes from the Cu_3P and it still traces the existence of $Cu_3(PO_4)_2$ on the catalyst surface in accordance with the results of Fig. 8A.

Fig. 9 depicts the valence band spectra (VB) of all samples taken by XPS. The VB consists mainly of one peak, located at *ca.* 3.3 eV, corresponding to Cu 3d [62]. The position of this peak is practically the same before and after reaction. However, the full width half maximum (FWHM) is larger for the fresh sample (spectrum a) due to the existence of OH species as discussed above. The VB maximum is very close to the Fermi level confirming the p-type character of Cu_3P.

3.5. Mechanistic implications

Results presented in Fig. 3A show that the homogeneous degradation of SMX in the presence of persulfate is very slow. However, the degradation rate increases drastically in the presence of copper
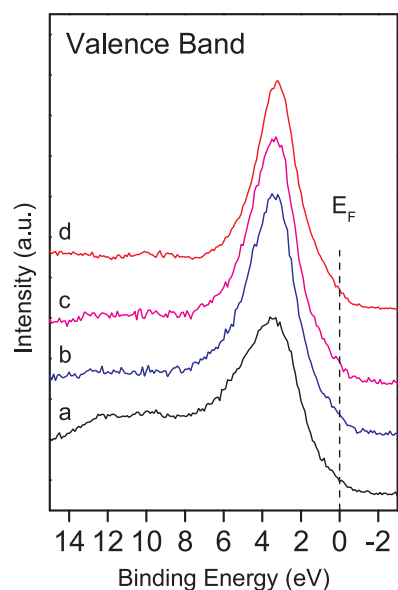
Fig. 9. X-ray photoelectron spectra in the valence band region obtained from (a) the fresh catalyst, and from spent catalyst samples collected after exposure to reaction conditions for (b) 4 min, (c) 8 min and (d) 120 min. Experimental conditions as in Fig. 8.
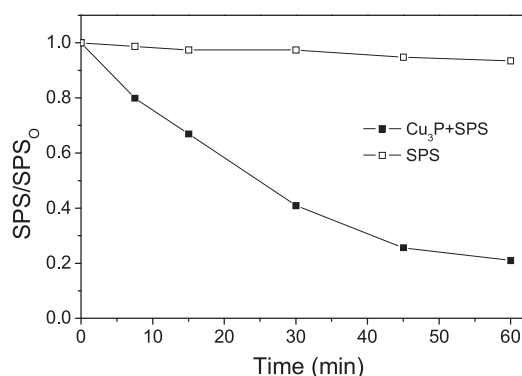

Fig. 10. SPS consumption (0.1 g/L) in the presence (filled symbols) and in the absence (open symbols) of 40 mg/L Cu_3P in UPW.

phosphide evidencing that this material is an efficient activator of SPS. This is also verified by results presented in Fig. 10, showing that SPS concentration (in the absence of SMX) decreases rapidly only in the presence of Cu_3P.

Results of XRD (Fig. 1) and XPS (Fig. 8) showed that (i) the catalyst consists of Cu_3P phase and (ii) its bulk and surface composition do not change under reaction conditions to form, for example, CuO_x or other unphosphided species (it should be reminded that the residual $Cu(OH)_2$ and $Cu_3(PO_4)_2$ species detected by XPS, which originate from the synthesis method employed, are rapidly removed from the surface of the freshly prepared catalyst under reaction conditions). The conclusion that the latter surface species are not responsible for the observed catalytic activity is verified by the fact that the used catalyst, which is free of $Cu(OH)_2$ and $Cu_3(PO_4)_2$, exhibits the same catalytic performance with the fresh sample (compare the solid and dashed lines obtained with 40 mg/L Cu_3P in Fig. 3A). This provides evidence that a heterogeneous reaction mechanism is operable in which Cu_3P participates as a stable catalyst/activator. Therefore, in contrast to conventional Fenton-type systems, where persulfate activation occurs by dissolved transition metals (e.g., Fe^{2+}, Mn^{2+}, Ag^+, Co^{2+}, Ni^{2+}) or on redox-active surface sites [63], the Cu_3P-activated reaction may be considered as a real catalytic process that does not involve changes in the catalyst

composition and/or oxidation state.

Results of the present work can be discussed considering the reaction mechanisms proposed in few recent studies, where activation of persulfate was achieved by non-conventional catalysts such as nano-carbons [64–66] and supported noble metal catalysts [67,68]. For example, Lee et al. [65] found that, in contrast to conventional systems, carbon nanotubes (CNTs) can activate persulfates via non-radical mechanisms to form reactive species that can effectively degrade organic compounds in solution. The authors concluded that the reaction mechanism involves electron transfer between the reactant (e.g. phenol, which is an electron donor), CNTs (an electron mediator), and persulfate (an electron acceptor). Qualitatively similar results were reported by Duan et al. [66] who applied several dimensional-structured nano-carbons as metal-free catalysts to activate SPS for the catalytic oxidation of phenolic compounds and dyes. The authors found that single-walled CNTs, reduced graphene oxide and mesoporous carbon exhibited high activity for heterogeneous SPS activation, which was superior to that of metal oxides such as Fe_3O_4, CuO, Co_3O_4 and MnO_2 [66]. Based on results of EPR experiments, they proposed that carbo-catalysts might act as an electron bridge in activation of SPS to oxidize adsorbed water directly to generate hydroxyl radicals [66].

Regarding supported noble-metal catalysts, Ahn et al. [67] showed that noble metals (Pd, Pt, Au, Ag) dispersed on Al_2O_3 or TiO_2 can effectively activate PMS to degrade organic compounds in water. Based on the fact that degradation kinetics depended on the nature of the organic substrate and were not affected by sulfate radical scavengers, they also concluded that the oxidation process over these catalysts does not involve $SO_4^{\cdot-}$ as oxidant. Results were explained considering a non-radical mechanism, where noble metals mediate electron transfer from organic compounds to PMS to achieve persulfate-driven oxidation [65]. In contrast, Feng et al. [68] who studied degradation of 1,4-dioxane with PMS over Pd/Al_2O_3 catalyst, reported a strong inhibitory effect of common scavengers on the degradation kinetics and proposed that surface-bound sulfate radicals were the dominant active species.

Based on the above, results of the present study can be explained taking into account the electronic characteristics of Cu_3P [69] and the redox potentials of the various species that may be formed under the present reaction conditions ([70] and refs. therein) (see Fig. 11). As discussed above, the synthesized Cu_3P catalyst is a p-type semiconductor (Fig. 9). According to the literature, this material has a band gap of *ca.* 1.6 eV, a valence band maximum (E_{VB}) of +1.02 V vs NHE and a conduction band minimum (E_{CB}) of -0.64 V vs, NHE [69]. Considering the relative positions of the above energy levels and the fact that $SO_4^{\cdot-}$ radicals were found to be the dominant oxidizing species under the present conditions (Fig. 6B), two different reaction pathways may be operable:
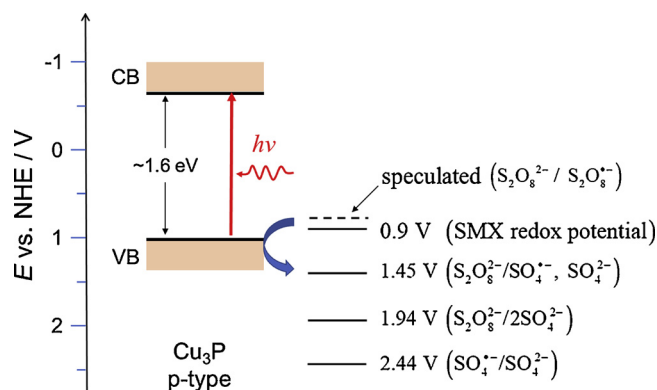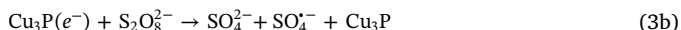

Fig. 11. Band-edge positions of Cu_3P and redox potentials of species involved in the title reaction.
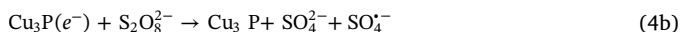
3.5.1. Reaction pathway I

The redox potential of SMX ($+0.9$ V vs NHE) [71] is located higher than the E_{VB} of Cu_3P (Fig. 11) and, therefore, SMX can be oxidized on the Cu_3P surface by donating an electron to the catalyst. The electron can then be transferred from the VB of Cu_3P to $S_2O_8^{2-}$ to produce $SO_4^{\cdot-}$ radicals (Fig. 11):

$$Cu_3P + SMX \rightarrow Cu_3P(e^-)\cdots[SMX]^+ \tag{3a}$$

$$Cu_3P(e^-) + S_2O_8^{2-} \rightarrow SO_4^{2-} + SO_4^{\cdot-} + Cu_3P \tag{3b}$$

This reaction pathway has some similarities with the one proposed by Lee et al. for persulfate activation over carbon nanotubes (CNTs) with the exception that it involves formation of radical species [65].

3.5.2. Reaction pathway II

The fact that Cu_3P can decompose SPS in the absence of SMX (Fig. 10) implies that activation of persulfate may occur via electron transfer to and from the Cu_3P catalyst according to the following reaction steps (Fig. 11):

$$Cu_3P + S_2O_8^{2-} \rightarrow Cu_3P(e^-) + S_2O_8^{\cdot-} \tag{4a}$$

$$Cu_3P(e^-) + S_2O_8^{2-} \rightarrow Cu_3P + SO_4^{2-} + SO_4^{\cdot-} \tag{4b}$$

As discussed by Liu et al. [63], the ability of persulfate to be both oxidized and reduced resembles the property of H_2O_2 to act as both an oxidant and reductant in the Fenton system. The overall reaction results in the formation of persulfate radicals ($S_2O_8^{\cdot-}$) and sulfate radicals ($SO_4^{\cdot-}$), and is similar to that proposed for the transition metal-catalyzed reaction:

$$2S_2O_8^{2-} \xrightarrow{Cu_3P} S_2O_8^{\cdot-} + SO_4^{2-} + SO_4^{\cdot-} \tag{5}$$

It should be noted that the latter reaction mechanism implies that the redox potential of the $S_2O_8^{2-}/S_2O_8^{\cdot-}$ couple (Eq. 4a) is located higher than the E_{VB} of Cu_3P. Unfortunately, this assumption cannot be supported by literature results because, to the best of our knowledge, this value is not available in the literature.

The $SO_4^{\cdot-}$ radicals produced via reactions (3b) and (4b) may then oxidize water to yield $^\cdot OH$ radicals that may also participate in the degradation process [15]:

$$SO_4^{\cdot-} + H_2O \rightarrow SO_4^{2-} + {}^\cdot OH + H^+ \tag{6}$$

Formation of $^\cdot OH$ is accompanied by the production of H^+ (Eq. 6), which explains the progressive decrease of the solution pH from *ca.* 6.5 to *ca.* 4.5 in experiments with UPW.

It should be noted that in both of the above reaction pathways, Cu_3P acts as an electron mediator or electron bridge to facilitate the fast electron-transfer processes [66,67]. The catalyst remains intact during the degradation of SMX and, therefore, the overall process is a real catalytic one. In both cases, the reaction involves intermediate formation of radicals, which is in general agreement with the mechanism proposed by Feng et al. over Pd/Al_2O_3 catalyst [68]. The main difference between the two proposed mechanisms is that "pathway I" involves the formation of a surface-bound intermediate (reaction 3a) and, therefore, may be substrate-specific. In contrast, "pathway II" should be non-selective and is expected to be operable for any organic compound in solution. These issues are beyond the scope of the present work and will be studied in detail in our future investigations.

4. Conclusions

Copper phosphide was synthesized, characterized and eventually tested in this work as an activator of persulfate salt for the degradation of antibiotic SMX in water matrices. To the best of our knowledge, this is the first report regarding the application of the SPS/Cu_3P pair for environmental applications.

1) Cu_3P, a p-type semiconductor, seems to act as an electron mediator capable of accelerating electron transfer processes in a way that leads to the intermediate formation of sulfate and other radicals. This is supported comparing the results of characterization between the fresh catalyst and spent samples collected at various reaction times; the catalyst remains intact without changes in its composition and oxidation state.

2) Fast degradation of SMX occurs in UPW and the rate depends on factors such as SMX, SPS and Cu_3P concentrations. Actual matrices such as bottled water and treated wastewater impose a detrimental effect on degradation compared to UPW; the bicarbonate ion appears to be the main responsible for this behavior.

3) Process integration is conceptually advantageous to enhance slow degradation rates. This is particularly true if coupling results in a synergistic rather than additive effect. In this work, synergy was achieved when SPS activation was simultaneously done by Cu_3P and artificial solar irradiation. The degree of synergy is more pronounced in those conditions, where degradation rates are low (i.e. in wastewater).

References

[1] H.V. Lutze, S. Bircher, I. Rapp, N. Kerlin, R. Bakkour, M. Geisler, C. von Sonntag, T.C. Schmidt, Degradation of chlorotriazine pesticides by sulfate radicals and the influence of organic matter, Environ. Sci. Technol. 49 (2015) 1673–1680.

[2] J. Wang, S. Wang, Activation of persulfate (PS) and peroxymonosulfate (PMS) and application for the degradation of emerging contaminants, Chem. Eng. J. 334 (2018) 1502–1517.

[3] Q. Huang, J. Zhang, Z. He, P. Shi, X. Qin, W. Yao, Direct fabrication of lamellar self-supporting Co_3O_4/N/C peroxymonosulfate activation catalysts for effective aniline degradation, Chem. Eng. J. 313 (2017) 1088–1098.

[4] Y. Liu, X. He, Y. Fu, D.D. Dionysiou, Degradation kinetics and mechanism of oxytetracycline by hydroxyl radical-based advanced oxidation processes, Chem. Eng. J. 284 (2016) 1317–1327.

[5] P. Drzewicz, L. Perez Estrada, A. Alpatova, J.W. Martin, M.G. El-Din, Impact of peroxydisulfate in the presence of zero valent iron on the oxidation of cyclohexanoic acid and naphthenic acids from oil sands process-affected water, Environ. Sci. Technol. 46 (2012) 8984–8991.

[6] G.P. Anipsitakis, D.D. Dionysiou, Degradation of organic contaminants in water with sulfate radicals generated by the conjunction of peroxymonosulfate with cobalt, Environ. Sci. Technol. 37 (20) (2003) 4790–4797.

[7] H.G. Gorchev, G. Ozolins, WHO guidelines for drinking-water quality, WHO Chron. 38 (3) (1984) 104–108.

[8] R.H. Waldemer, P.G. Tratnyek, R.L. Johnson, J.T. Nurmi, Oxidation of chlorinated ethenes by heat-activated persulfate: kinetics and products, Environ. Sci. Technol. 41 (2007) 1010–1015.

[9] Y. Gao, N. Gao, Y. Deng, Y. Yang, Y. Ma, Ultraviolet (UV) light-activated PS oxidation of sulfamethazine in water, Chem. Eng. J. 195–196 (2012) 248–253.

[10] G.P. Anipsitakis, D.D. Dionysiou, Radical generation by the interaction of transition metals with common oxidants, Environ. Sci. Technol. 38 (2004) 3705–3712.

[11] C. Qi, X. Liu, J. Ma, C. Lin, X. Li, H. Zhang, Activation of PMS by base: implications for the degradation of organic pollutants, Chemosphere 151 (2016) 280–288.

[12] X. Lou, C. Fang, Z. Geng, Y. Jin, D. Xiao, Z. Wang, J. Liu, Y. Guo, Significantly enhanced base activation of peroxymonosulfate by polyphosphates: kinetics and mechanism, Chemosphere 173 (2017) 529–534.

[13] Q. Yang, H. Choi, D.D. Dionysiou, Nanocrystalline cobalt oxide immobilized on titanium dioxide nanoparticles for the heterogeneous activation of peroxymonosulfate, Appl. Catal. B: Environ. 74 (2007) 170–178.

[14] P.R. Shukla, S. Wang, H. Sun, H.M. Ang, M. Tadé, Activated carbon supported cobalt catalysts for advanced oxidation of organic contaminants in aqueous solution, Appl. Catal. B: Environ. 100 (2010) 529–534.

[15] H. Zhang, X. Liu, J. Ma, C. Lin, C. Qi, X. Li, Z. Zhou, G. Fan, Activation of peroxymonosulfate using drinking water treatment residuals for the degradation of

atrazine, J. Hazard. Mater. 344 (2018) 1220–1228.

[16] S.H. Yuan, P. Liao, A.N. Alshawabkeh, Electrolytic manipulation of persulfate re-activity by iron electrodes for trichloroethylene degradation in groundwater, Environ. Sci. Technol. 48 (2014) 656–663.

[17] F.F. Hao, L.L. Guo, A.Q. Wang, Y.Q. Leng, H.L. Li, Intensification of sonochemical degradation of ammonium perfluooctanoate by persulfate oxidant, Ultrason. Sonoshem. 21 (2014) 554–558.

[18] J. Paul, D.B. Naik, Y.K. Bhardwaj, L. Varshney, Studies on oxidative radiolysis of ibuprofen in presence of potassium persulfate, Radiat. Phys. Chem. 100 (2014) 38–44.

[19] J. Criquet, N.K.V. Leitner, Reaction pathway of the degradation of the phydrox-ybenzoic acid by sulfate radical generated by ionizing radiations, Radiat. Phys. Chem. 106 (2015) 307–314.

[20] J. Deng, C. Ya, Y. Ge, Y. Cheng, Y. Chen, M. Xu, H. Wang, Activation of perox-ymonosulfate by metal (Fe, Mn, Cu and Ni) doping ordered mesoporous Co_3O_4 for the degradation of enrofloxacin, RSC Adv. 8 (2018) 2338–2349.

[21] B.-T. Zhang, Y. Zhang, Y. Teng, M. Fan, Sulfate radical and its application in de-contamination technologies, Crit. Rev. Environ. Sci. Technol. 45 (2015) 1756–1800.

[22] P. Shukla, S. Wang, K. Singh, H.M. Ang, M.O. Tadé, Cobalt exchanged zeolites for heterogeneous catalytic oxidation of phenol in the presence of perox-ymonosulphate, Appl. Catal. B: Environ. 99 (2010) 163–169.

[23] Q. Yang, H. Choi, Y. Chen, D.D. Dionysiou, Heterogeneous activation of perox-ymonosulfate by supported cobalt catalysts for the degradation of 2,4-di-chlorophenol in water: the effect of support, cobalt precursor, and UV radiation, Appl. Catal. B: Environ. 77 (2008) 300–307.

[24] W. Zhang, H.L. Tay, S.S. Lim, Y. Wang, Z. Zhong, R. Xu, Supported cobalt oxide on MgO: highly efficient catalysts for degradation of organic dyes in dilute solutions, Appl. Catal. B: Environ. 95 (2010) 93–99.

[25] T. Zhang, Y. Chen, Y. Wang, J. Le Roux, Y. Yang, J.-P. Croué, Efficient perox-ydisulfate activation process not relying on sulfate radical generation for water pollutant degradation, Environ. Sci. Technol. 48 (10) (2014) 5868–5875.

[26] Y. Lei, C.-S. Chen, Y.-J. Tu, Y.-H. Huang, H. Zhang, Heterogeneous degradation of organic pollutants by persulfate activated by $CuO-Fe_3O_4$: mechanism, stability, and effects of pH and bicarbonate ions, Environ. Sci. Technol. 49 (11) (2015) 6838–6845.

[27] X. Dua, Y. Zhanga, I. Hussaina, Huanga S, W. Huange, Insight into reactive oxygen species in persulfate activation with copper oxide: activated persulfate and trace radicals, Chem. Eng. J. 313 (2017) 1023–1032.

[28] J.F. Callejas, C.G. Read, C.W. Roske, N.S. Lewis, R.E. Schaak, Synthesis, char-acterization, and properties of metal phosphide catalysts for the Hydrogen-Evolution Reaction, Chem. Mater. 28 (2015) 6017–6044.

[29] S. Ni, J. Ma, X. Lv, X. Yang, L. Zhang, The fine electrochemical performance of porous Cu_3P/Cu and the high energy density of Cu_3P as anode for Li-ion batteries, J. Mater. Chem. A 2 (2014) 20506–20509.

[30] S.T. Oyama, T. Gatt, H. Zhao, Y.-K. Lee, Transition metal phosphide hydroproces-sing catalysts: a review, Catal. Today 143 (2009) 94–107.

[31] L. Ma, X. Shen, H. Zhou, J. Zhu, C. Xi, Z. Ji, L. Kong, Synthesis of Cu_3P nanocubes and their excellent electrocatalytic efficiency for the hydrogen evolution reaction in acidic solution, RCS Adv. 6 (2016) 9672–9677.

[32] X. Yue, S. Yi, R. Wang, Z. Zhang, S. Qiu, Novel earth-abundant Cu_3P with TiO_2 architectured high efficient "p-n" heterojunction nanophotocatalyst for water splitting hydrogen evolution, Nanoscale 8 (2016) 17516–17523.

[33] Z. Qin, M. Wang, R. Li, Y. Chen, Novel $Cu_3P/g-C_3N_4$ p-n heterojunction photo-catalysts for solar hydrogen generation, Sci. China Mater. 61 (2018) 861–868.

[34] Z. Sun, Q. Yue, J. Li, J. Xu, H. Zheng, P. Du, Copper phosphide modified cadmium sulfide nanorods as a novel p–n heterojunction for highly efficient visible-light-driven hydrogen production in water, J. Mater. Chem. A 3 (2015) 10243–10247.

[35] R. Luo, C. Liu, J. Li, J. Wang, X. Hu, X. Sun, J. Shen, W. Han, L. Wang, Nanostructured CoP: an efficient catalyst for degradation of organic pollutants by activating peroxymonosulfate, J. Hazard. Mater. 329 (2017) 92–101.

[36] A. Ioannidi, Z. Frontistis, D. Mantzavinos, Destruction of propyl paraben by per-sulfate activated with UV-A light emitting diodes, J. Environ. Chem. Eng. 6 (2018) 2992–2997.

[37] Y. Kanigaridou, A. Petala, Z. Frontistis, M. Antonopoulou, M. Solakidou, I. Konstantinou, Y. Deligiannakis, D. Mantzavinos, D.I. Kondarides, Solar photo-catalytic degradation of bisphenol A with $CuO_x/BiVO_4$: insights into the un-expectedly favorable effect of bicarbonates, Chem. Eng. J. 318 (2017) 39–49.

[38] B.D. Cullity, J.W. Weymouth, Elements of X-Ray diffraction, Am. J. Phys. 25 (1957) 394–395.

[39] C. Liang, C.-F. Huang, N. Mohanty, R.M. Kurakalva, A rapid spectrophotometric determination of persulfate anion in ISCO, Chemosphere 73 (2008) 1540–1543.

[40] S. Cao, Y. Chen, C.-J. Wang, X.-J. Lv, W.-F. Fu, Spectacular photocatalytic hydrogen evolution using metal-phosphide/CdS hybrid catalysts under sunlight irradiation, Chem. Commun. 51 (2015) 8708–8711.

[41] R.L. Siegrist, M. Crimi, T.J. Simpkin, In situ chemical oxidation for groundwater remediation, SERDP ESTCP Environmental Remediation Technology Vol. 3 Springer Science + Business Media, LLC, New York, 2011.

[42] A. Jawad, J. Lang, Z. Liao, A. Khan, J. Ifthikar, Z. Lv, S. Long, Z. Chen, Z. Chen, Activation of persulfate by $CuO_x@Co-LDH$: a novel heterogeneous system for con-taminant degradation with broad pH window and controlled leaching, Chem. Eng. J. 335 (2018) 548–559.

[43] C. Cai, L. Wang, H. Gao, L. Hou, H. Zhang, Ultrasound enhanced heterogeneous activation of peroxydisulfate by bimetallic Fe-Co/GAC catalyst for the degradation of Acid Orange 7 in water, J. Environ. Sci. 26 (2014) 1267–1273.

[44] R.H. Waldemer, P.G. Tratnyek, R.L. Johnson, J.T. Nurmi, Oxidation of chlorinated ethenes by heat-activated persulfate: kinetics and products, Environ. Sci. Technol.

[45] X. Zhang, M. Feng, R. Qu, H. Liu, L. Wang, Z. Wang, Catalytic degradation of diethyl phthalate in aqueous solution by persulfate activated with nano-scaled magnetic $CuFe_2O_4/MWCNTs$, Chem. Eng. J. 301 (2016) 1–11.

[46] Y. Wu, Y. Shi, H. Chen, J. Zhao, W. Dong, Activation of persulfate by magnetite: implications for the degradation of low concentration sulfamethoxazole, Process Saf. Environ. 116 (2018) 468–476.

[47] J. Du, W. Guo, D. Che, N. Ren, Weak magnetic field for enhanced oxidation of sulfamethoxazole by Fe^o/H_2O_2 and $Fe^o/persulfate$: performance, mechanisms, and degradation pathways, Chem. Eng. J. 351 (2018) 532–539.

[48] H. Chen, K.C. Carroll, Metal-free catalysis of persulfate activation and organic-pollutant degradation by nitrogen-doped graphene and aminated graphene, Environ. Pollut. 215 (2016) 96–102.

[49] S. Zhu, X. Huang, F. Ma, L. Wang, X. Duan, S. Wang, Catalytic removal of aqueous contaminants on N-doped graphitic biochars: inherent roles of adsorption and nonradical mechanisms, Environ. Sci. Technol. 52 (2018) 8649–8658.

[50] L. Kemmou, Z. Frontistis, J. Vakros, I.D. Manariotis, D. Mantzavinos, Degradation of antibiotic sulfamethoxazole by biochar-activated persulfate: factors affecting the activation and degradation processes, Catal. Today 313 (2018) 128–133.

[51] D. Dimitrakopoulou, I. Rethemiotaki, Z. Frontistis, N.P. Xekoukoulotakis, D. Venieri, D. Mantzavinos, Degradation, mineralization and antibiotic inactivation of amoxicillin by UV-A/TiO_2 photocatalysis, J. Environ. Manage. 98 (2012) 168–174.

[52] C. Luo, J. Jiang, J. Ma, S. Pang, Y. Liu, Y. Song, C. Guan, J. Li, Y. Jin, D. Wu, Oxidation of the odorous compound 2,4,6-trichloroanisole by UV activated per-sulfate: kinetics, products and pathways, Water Res. 96 (2016) 12–21.

[53] J. Ma, H. Li, Y. Yang, X. Li, Influence of water matrix species on persulfate oxidation of phenol: reaction kinetics and formation of undesired degradation byproducts, Water Sci. Technol. 2017 (2) (2018) 340–350, https://doi.org/10.2166/wst.2018. 147.

[54] J.-F. Yang, L.-M. Yang, S.-B. Zhang, L.-H. Ou, C.-B. Liu, L.-Y. Zheng, Y.-F. Yang, G.-G. Ying, S.-L. Luo, Degradation of azole fungicide fluconazole in aqueous solution by thermally activated persulfate, Chem. Eng. J. 321 (2017) 113–122.

[55] M.E. Metheniti, Z. Frontistis, R.S. Ribeiro, A.M.T. Silva, J.L. Faria, H.T. Gomes, D. Mantzavinos, Degradation of propyl-paraben by activated persulfate using iron-containing magnetic carbon xerogels: investigation of water matrix and process synergy effects, Environ. Sci. Pollut. Res. (2017), https://doi.org/10.1007/s11356-017-0178-9.

[56] Y. Yang, J. Jiang, X. Lu, J. Ma, Y.Z. Liu, Production of sulfate radical and hydroxyl radical by reaction of ozone with peroxymonosulfate: a novel advanced oxidation process, Environ. Sci. Technol. 49 (2015) 7330–7339.

[57] G. Fang, J. Gao, D.D. Dionysiou, C. Liu, D. Zhou, Activation of persulfate by qui-nones: free radical reactions and implication for the degradation of PCBs, Environ. Sci. Technol. 47 (2013) 4605–4611.

[58] Y. Xu, H. Lin, Y. Li, H. Zhang, The mechanism and efficiency of MnO_2 activated persulfate process coupled with electrolysis, Sci. Total Environ. 609 (2017) 644–654.

[59] M.C. Biesinger, L.W.M. Lau, A.R. Gerson, R.S.C. Smart, Resolving surface chemical states in XPS analysis of first row transition metals, oxides and hydroxides: Sc, Ti, V, Cu and Zn, Appl. Surf. Sci. 257 (3) (2010) 887–898.

[60] G.D. Khattak, M.A. Salim, L.E. Wenger, A.H. Gilani, X-ray photoelectron spectro-scopy (XPS) and magnetic susceptibility studies of copper-vanadium phosphate glasses, J. Non-Cryst. Solids 262 (1) (2000) 66–79.

[61] S.W. Gaarenstroom, N. Winograd, Initial and final state effects in the ESCA spectra of cadmium and silver oxides, J. Chem. Phys. 67 (8) (1977) 3500–3506.

[62] V.I. Nefedov, Y.V. Salyn, E.P. Domashevskaya, Y.A. Ugai, V.A. Terekhov, A study by XPS and XRS of the participation in chemical bonding of the 3d electrons of copper, zinc and gallium, J. Electron Spectros. Relat. Phenomena 6 (3) (1975) 231–238.

[63] H. Liu, T.A. Bruton, F.M. Doyle, D.L. Sedlak, In situ chemical oxidation of con-taminated groundwater by persulfate: decomposition by Fe(III)- and Mn(IV)-con-taining oxides and aquifer materials, Environ. Sci. Technol. 48 (2014) 10330–10336.

[64] H. Sun, C.K. Kwan, A. Suvorova, H.M. Ang, M.O. Tadé, S. Wang, Catalytic oxidation of organic pollutants on pristine and surfacenitrogen-modified carbon nanotubes with sulfate radicals, Appl. Catal. B: Environ. 154–155 (2014) 134–141.

[65] H. Lee, H.-J. Lee, J. Jeong, J. Lee, N.-B. Park, C. Lee, Activation of persulfates by carbon nanotubes: oxidation of organic compounds by nonradical mechanism, Chem. Eng. J. 266 (2015) 28–33.

[66] X. Duan, H. Sun, J. Kang, Y. Wang, S. Indrawirawan, S. Wang, Insights into het-erogeneous catalysis of persulfate activation on dimensional-structured nano-carbons, ACS Catal. 5 (2015) 4629–4636.

[67] Y.-Y. Ahn, E.-T. Yun, J.-W. Seo, C. Lee, S.H. Kim, J.-H. Kim, J. Lee, Activation of peroxymonosulfate by surface-loaded noble metal nanoparticles for oxidative de-gradation of organic compounds, Environ. Sci. Technol. 50 (2016) 10187–10197.

[68] Y. Feng, P.-H. Lee, D. Wu, K. Shih, Surface-bound sulfate radical-dominated de-gradation of 1,4-dioxane by alumina-supported palladium (Pd/Al_2O_3) catalyzed peroxymonosulfate, Water Res. 120 (2017) 12–21.

[69] A. Rauf, M. Ming, S. Kim, Md.S.A.A.Sher Shah, C.-H. Chung, J.H. Park, P.J. Yoo, Mediator and co-catalysts-free direct Z-scheme composites of $Bi_2WO_6-Cu_3P$ for solar-water splitting, Nanoscale 10 (2018) 3026–3036, https://doi.org/10.1039/C7NR07952D.

[70] J.K. Hurst, M.D. Roemeling, S.V. Lymar, Mechanistic insight into peroxydisulfate reactivity: Oxidation of the cis,cis-$[Ru(bpy)_2(OH_2)]_2O^{4+}$ "Blue Dimer", J. Phys. Chem. B 119 (2015) 7749–7760.

[71] L. Zhou, G. Zou, H. Deng, The roles of graphene and Ag in the hybrid Ag@Ag_2O-graphene for sulfamethoxazole degradation, Catalysts 8 (2018) 272.